

Hydrothermal Venting Along Earth’s Fastest Spreading Center: East Pacific Rise, 27.5°–32.3°S

E. T. Baker,¹ R. N. Hey,² J. E. Lupton,³ J. A. Resing,⁴ R. A. Feely,¹ J. J. Gharib,⁵ G. J. Massoth,^{1,9} F. J. Sansone,⁵ M. Kleinrock,⁶ F. Martinez,² D. F. Naar,⁷ C. Rodrigo,⁸ D. Bohnenstiehl,^{6,10} and D. Pardee²

Abstract. During March/April 1998 we conducted detailed mapping and sampling of hydrothermal plumes along six segments of Earth’s fastest spreading midocean ridge, 27.5°–32.3°S on the East Pacific Rise. We compared the distribution and chemistry of hydrothermal plumes to geological indicators of long-term (spreading rate) and moderate-term (ridge inflation) variations in magmatic budget. In this large-offset, propagating rift setting, these geological indices span virtually the entire range found along fast-spreading ridges worldwide. Hydrothermal plumes overlaid ~60% of the length of superfast (>130 km/Myr) spreading axis surveyed, comparable to earlier results from 13.5°–18.7°S on the East Pacific Rise, and defined at least 14 separate vent fields. We observed no plumes over the slower-spreading propagating segments. Finer-scale variations in the magmatic budget also correlated with hydrothermal activity, as the location of the five most intense plumes corresponded to subsegment peaks in ridge inflation. Along the entire ridgecrest, the more inflated a ridge location the more likely it was to be overlain by a hydrothermal plume. Plume chemistry mostly reflected discharge from mature vent fields apparently unperturbed by magmatic activity within the last few years. Plume samples with high volatile/metal ratios, generally indicating recent seafloor volcanism, were scarce. Along-axis trends in both volatile ($\Delta^3\text{He}$; CH_4 ; ΔpH , a proxy for CO_2 ; and particulate S) and non-volatile (Fe, Mn) species showed a first-order agreement with the trend of ridge inflation. Nevertheless, a broad correspondence between the concentration of volatile species in plumes and geological proxies of magma supply identifies a pervasive magmatic imprint on this superfast-spreading group of ridge segments.

1. Introduction

The Pacific-Nazca Ridge between the Easter and

¹Pacific Marine Environmental Laboratory, NOAA, Seattle, Washington

²Hawaii Institute of Geophysics and Planetology, University of Hawaii, Honolulu

³Pacific Marine Environmental Laboratory, NOAA, Newport, Oregon

⁴Joint Institute for the Study of the Atmosphere and Ocean, University of Washington, Seattle

⁵Department of Oceanography, University of Hawaii, Honolulu

⁶Department of Geology, Vanderbilt University, Nashville, Tennessee

⁷Department of Marine Science, University of South Florida, St. Petersburg

⁸Servicio Hidrografico y Oceanografico de la Armada Valparaiso, Chile

⁹Present address: Institute of Geological and Nuclear Sciences, Ltd., Lower Hutt, New Zealand

¹⁰Present address: Lamont-Doherty Earth Observatory, Palisades, New York

Copyright by the American Geophysical Union.

Paper number .
0148-0227/02/\$9.00

Juan Fernandez microplates includes the planet's fastest-spreading ridge segments and largest active set of dueling propagators, with an along- and across-axis scale of ~ 120 km (Figure 1) [Hey *et al.*, 1995]. This large-offset propagating rift is reorganizing the local plate boundary geometry and perhaps represents an initial stage in the formation of a new microplate [Hey *et al.*, 1995]. Such rapid plate boundary evolution creates steep regional gradients in the magmatic budget that are reflected in the geological characteristics of each ridge segment. For example, the long-term (>1 Myr) magmatic budget, indicated by the spreading rate (u_s), spans the full global extent, from 0 to 150 km/Myr. Shorter-period (~ 0.1 Myr) fluctuations in the magmatic budget, tracked by sub-segment-scale variability in the ridge crest cross-sectional area (A_{xs}), also cover nearly the entire range found along the East Pacific Rise (EPR) [Scheirer and Macdonald, 1993; Martínez *et al.*, 1997].

Because of this diversity, the region is an ideal natural laboratory for exploring the influence of fluctuations in the magmatic budget on the distribution and composition of hydrothermal venting. The only previous detailed study of hydrothermal plumes along a superfast ridge was conducted in 1993 along the "Ridge Flux" area—the southern EPR between 13.5° and 18.7° S [Urabe *et al.*, 1995; Baker and Urabe, 1996; Feely *et al.*, 1996; Ishibashi *et al.*, 1997]. Plume mapping and sampling there found abundant plumes, a moderate correlation between the cross-sectional area of segments and plume presence, and a marked variability in plume chemical composition that distinguished sites of recent magmatic activity from more hydrothermally mature sites. However, the relatively small range in proxies of both long (u_s) and moderate-term (A_{xs}) magmatic budgets at that site limit the inferences that can be drawn about the importance of magmatic budget fluctuations in controlling hydrothermal discharge.

To overcome that limitation, we conducted a detailed hydrothermal and geophysical study of the EPR between the Easter and Juan Fernandez microplates during March/April 1998. The RAPA NUI study area extends from 27.5° to 32.3° S and includes six second-order tectonic segments (Figure 1). Our primary objectives were to examine three specific questions that address the influence of geological controls on hydrothermal venting at different spatial and temporal scales:

1. Is the spatial density of hydrothermal venting relatively greater along a plate boundary undergoing reorganization than along segments of similar morphology and spreading rate along a stable boundary? Layers of metalliferous sediments found in Deep-Sea Drilling Program cores in the southeast Pacific suggest that previous plate boundary reorganizations have triggered unusually intense hydrothermal activity [Owen and Rea, 1987; Lyle *et al.*, 1987]. The morphological similarity of segments in the 1998 RAPA NUI survey to segments previously surveyed along the stable Ridge Flux plate boundary [Baker and Urabe, 1996] allows a direct comparison between superfast unstable and stable plate boundaries.

2. How closely does the distribution of hydrothermal discharge correspond to segment and sub-segment variations in the apparent magmatic budget? These variations, expressed as changes in A_{xs} , are thought to have a time scale on the order of 0.1 Myr, presumably a much longer time scale than the expected lifetime of hydrothermal fields (~ 10

to 100 years) on fast-spreading ridges [Auzende *et al.*, 1996; Hooft *et al.*, 1997]. Prior regional-scale studies have come to conflicting conclusions on the soundness of any correlation between $A_{x.s}$ and hydrothermal activity [Baker, 1996; Hooft *et al.*, 1997]. These interpretations suffer, however, from the limited extent of ridge crest so far examined, the small range of $A_{x.s}$ in the surveyed ridge sections, and the statistical approach used in the comparisons. The RAPA NUI area has a broader range of u_s and $A_{x.s}$ than sections of the EPR previously surveyed, allowing us to better isolate the relative effects on hydrothermal venting of variations of the magmatic budget at different time scales.

3. Does the high rate of magma delivery at superfast-spreading ridges produce frequent occurrences of volatile-rich hydrothermal fluids, symptomatic of magmatic perturbations? French submersible dives in 1993 between 17° and 19°S sampled five vents with volatile-rich fluids [Charlou *et al.*, 1996], and plume sampling during the 1993 Ridge Flux survey identified at least three locations discharging volatile-rich fluids apparently modified by recent magmatic activity [Urabe *et al.*, 1995]. The RAPA NUI survey doubled the length of the plume-sampled superfast-spreading ridge, enabling a more representative assessment of the hydrothermal chemistry produced at extreme magma supply rates.

2. Geologic Setting

The 610 km of EPR surveyed during this study includes six tectonic segments that define the dueling propagator between the Easter and Juan Fernandez microplates (Figure 1). The west ridge has been lengthening over the past 1.5–2 Myr, propagating south at about 135 km/Myr and gradually replacing east ridge segments [Naar and Hey, 1991; Hey *et al.*, 1995; Korenaga and Hey, 1996; Martínez *et al.*, 1997]. The high inflation and southward propagation of this ridge suggest it is influenced by the Easter Hotspot [Schilling *et al.*, 1985; Hey *et al.*, 1995]. Four segments make up the west ridge [Martínez *et al.*, 1997], but our survey included only the southerly two, W3 and W4. The full spreading rate is 148 km/Myr from 27.5°S (the start of our survey) to ~28.6°, and then declines steadily to effectively zero at the tip of W4 (Figure 2). The net elevation and $A_{x.s}$ (see Appendix 1) are higher on W3 than anywhere else in the survey area, and both show considerable intra- and inter-segment variability. W3 is bounded by two large OSCs, both with overlap lengths of ~20 km.

The east ridge includes four segments defined by small-offset OSCs and bounded on the south by another large OSC (Figure 2). The full spreading rate along segments E2–E4 is also a steady 148 km/Myr, decreasing to zero at the tip of E1. While the net elevation is nearly uniform along E2–E4, $A_{x.s}$ shows significant highs and lows. Martínez *et al.* [1997] conclude that the entire ridge is underlain by a single upwelling center, with shallow lateral magma transport maintaining the nearly constant depth of segments E2–E4. E1, the propagating tip, is the segment most dependent on along-axis magma transport and thus suffers periods of magma starvation as ridge location changes during a propagation event. The west ridge propagating segment, W4, likely undergoes similar cycles of magma supply and starvation.

3. Regional Distribution of Hydrothermal Activity

Contour plots of hydrothermal temperature ($\Delta\theta$) and light-scattering (ΔNTU) anomalies (see Appendix 1) map the distribution of major and minor plumes along the west and east ridges (Figure 3). The plume distribution recorded by MAPRs fixed to the DSL-120 tow cable was similar in all important respects to the results obtained using the CTDO package in the tow-yo mode (Walker et al., submitted). Most vent fields are identified equally well by either $\Delta\theta$ or ΔNTU , though in some cases the relative intensities of the two are quite different (e.g., near 28.2°S on W3, near 30.7° on E1, and along the southern end of E3). The complete lack of a particle signal corresponding to certain $\Delta\theta$ maxima (e.g., at the northern ends of W3 and E1) identifies places where substantial changes in the local hydrography produce non-hydrothermal $\Delta\theta$ increases.

Based on the CTDO tows, major vent fields exist on both the west and east ridges. On the west ridge, we found indications of the most energetic venting in the study area, based on a plume rise height >300 m at 28.45°S near the center of plume activity that stretched for more than 20 km along axis (Figure 3). We mapped a plume region of similar dimensions and intensity on the east ridge centered near 31.9°S on E4 (Figure 3). Within the overlap zone of the propagating tips (between 28.8° and 29.75°S), where u_s for each ridge falls below 130 km/Myr, hydrothermal plumes were absent on both the CTDO and MAPR surveys.

We summarize the regional spatial density of plumes by calculating plume incidence (p_h), the fraction of linear ridge axis overlain by a plume with ΔNTU greater than a threshold value of 0.015 V. We use ΔNTU rather than $\Delta\theta$ because particle settling and degradation restrict the spatial extent of the ΔNTU tracer more than the $\Delta\theta$ tracer, thereby giving a truer representation of the axial extent of the plume source locations. For the entire length of both the west and east ridges, p_h is 0.45. For those portions of both ridges where $u_s > 130$ km/Myr (north of 28.85°S on the west ridge and south of 29.75° on the east ridge) p_h rises to 0.62, similar to the value of 0.6 determined from the superfast-spreading Ridge flux area [Baker and Urabe, 1996]. (Note that we calculate these values from the raw data before contouring.) Thus the regional distribution of hydrothermal plumes confirms the results from the 1993 Ridge Flux survey [Urabe et al., 1995; Baker and Urabe, 1996] and supports a generalized model predicting a linear correlation between p_h and u_s [Baker et al., 1996].

The agreement in p_h between these two regions of the EPR demonstrates that, at least at present, the unstable plate boundary surveyed here is no more hydrothermally active than the stable boundary to the north (13.5°–18.7°S). In particular, the most unstable portions of the boundary, the propagating tips, are devoid of hydrothermal activity. A submersible search for hydrothermal activity at the tip of the 95.5°W propagator on the Galapagos Spreading Center similarly found scant evidence of hydrothermal activity [Hey et al., 1992]. Martínez et al. [1997] describe segment E1 of the east ridge as a volcanic constructional feature created ~0.2 Myr ago by magma erupting from a fracture in the brittle lithosphere during a propagation episode. Gravity and bathymetric data indicate a magma source from the inflated segments to the south rather than an under-

lying crustal reservoir, implying no persistent heat source to power hydrothermal activity. Hydrothermal venting at the tips of a propagator is thus likely to be intense during magmatic infilling of an advancing fracture, but very short lived.

4. Sub-segment-scale Distributions of Hydrothermal Activity

A specific objective of this survey was to compare sub-segment-scale hydrothermal activity (from the plume perspective) to indicators of the apparent magmatic budget, principally ridge inflation. Hydrothermal surveys over other Pacific ridges suggest that the mean A_{x_s} of individual second- to third-order tectonic segments generally correlates with their degree of hydrothermal activity [Baker, 1996]. Despite this positive correlation there was no simple functional relationship between p_h and the mean segment value of A_{x_s} . Rather, the data suggested a bimodal distribution of segments. Those with low values of A_{x_s} , indicative of a weak magmatic budget, had uniformly low p_h values. Those with values above a threshold level of $\sim 3.5 \text{ km}^2$, had p_h values ranging from low to 1. Part of the complexity of this relationship no doubt arises from the use of segment-mean values of A_{x_s} and p_h , particularly since the within-segment variability of both A_{x_s} and plume extent can be substantial.

Hooft *et al.* [1997] examined this relationship at a finer scale, comparing A_{x_s} and plume optical intensity along the EPR between 14° and 18°S at 0.03° intervals ($\sim 3 \text{ km}$). They found little correlation between the two and concluded that short-term permeability variations created by magmatic and tectonic events, not longer-term variability in the pooling of magma in the shallow crust, was the controlling factor in the distribution of hydrothermal activity.

One of the principal advantages of the present survey area in examining this relationship is its wide range in morphological characteristics. In particular, the range of A_{x_s} values is more than twice that at other plume-surveyed sites on the EPR (e.g., 9° – 12°N [Baker *et al.*, 1994], 13.5° – 18.7°S [Baker and Urabe, 1996]). A qualitative comparison of along-axis trends of A_{x_s} and hydrothermal activity, expressed as ΔNTU gridded at intervals of 0.03° and vertically integrated between the sea floor and the top of the local plume ($\Sigma\Delta\text{NTU}$), shows that plume maxima were coincident with peaks in ridge inflation (Figure 4). The slight offset of some plume peaks, such as near 28.5°S , presumably results from current-induced oscillation of a plume around its source. The location of plumes mapped during CTDO tow-yos and DSL-120 tows migrated by as much as 10 km when the time interval between each survey was as long as 5–6 days (Walker *et al.*, submitted). Despite this uncertainty in plume source location, we found the five most intense plumes (centered at 27.75° , 28° , 28.4° , 30.12° , and 31.9°S) to overlie short-wavelength peaks in A_{x_s} . (Data from the CTDO tow-yo shows the 28.4°S peak slightly offset to the north from the A_{x_s} peak at 28.5°S (Figure 4), but the $\Sigma\Delta\text{NTU}$ peak from the DSL-120/MAPR tow at this location precisely overlies the A_{x_s} peak (Walker *et al.*, submitted)). A similar agreement might also be inferred from the 1993 Ridge Flux data (Figure 4), but the smaller variability of A_{x_s} along that ridge section makes it difficult to identify an agreement with certainty.

For both study areas, plotting fine-scale (0.03° interval)

values of A_{xs} against $\Sigma\Delta NTU$ finds no functional relationship (Figure 5), the same result described by *Hoofst et al.* [1997]. But we expect a poor relationship on such a fine scale for two reasons. First, by virtue of their size and mobility plumes extend over much more of the axis than do the vent fields that produce them. Second, there is no a priori reason why the magnitude of any sampled plume tracer should correlate with A_{xs} . Nevertheless, these results still show that hydrothermal plumes are far more likely to be found over inflated sections of ridge, where $A_{xs} \gtrsim 3.5 \text{ km}^2$.

Since the correlation between ridge morphology and venting on either a segment or kilometer scale is poor, we take a more statistical approach by grouping the A_{xs} data in bins of 1 km^2 , regardless of location. For each 0.03° interval of ridge axis we determine (1) if a significant ($\Delta NTU \geq 0.015$) plume is present, and (2) which A_{xs} bin that interval occupies. We then plot the percentage of plume-covered intervals in each bin against the bin midpoint value (Figure 6). While each of the plume-surveyed SEPR areas show a strong correlation between plume percentage and A_{xs} , an especially good correlation exists for the combined data set, with $r^2 = 0.94$. This analysis confirms that even on the sub-segment scale the apparent magmatic budget is a first-order predictor of the likelihood of hydrothermal activity on these segments.

Even with this encouraging analysis, we have little better than a 50–50 chance of successfully predicting the occurrence of a hydrothermal plume along the bulk of these ridge segments, where A_{xs} values are 3–4 km^2 (Figure 6). To improve our prediction we need specific information on the other principal control on hydrothermal activity, permeability. For example, a recent study of two morphologically contrasting segments on the northern EPR found plumes scarce over a highly inflated and unfractured segment just north of the Orozco fracture zone, but plentiful over a narrow and heavily faulted adjacent segment [*Baker et al.*, 2001b]. Thus on some fast-spreading segments permeability seems to exert a more dominant influence on hydrothermal activity than does magmatic robustness. We suspect that the balance between these two factors lies in the temporal and spatial scales of alternation between the magmatic and tectonic phases of a given segment. The frequency of this alternation likely increases with increasing spreading rate [e.g., *Wilcock and Delaney*, 1996]. An important direction of future research will be determining the relative importance of magma budget and permeability as a function of spreading rate.

Similar multi-segment studies of hydrothermal discharge and fine-scale geology have been infrequent. *Wright et al.* [1995] found a consistent relationship between the depth and abundance of fissures and the population of hydrothermal vents between 9.2° and 9.6°N on the EPR. *Hoofst et al.* [1997], using the occurrence of an axial summit graben/caldera as a proxy for permeability in their study area, concluded that increased permeability was the principal contributing factor to hydrothermal activity. Their graben/caldera identification was based only on ship-borne multibeam bathymetry collected 10 yr before the hydrothermal observations; this temporal offset may be significant. In the RAPA NUI area, we used the DSL-120 deep tow package to collect continuous 120 kHz sidescan and bathymetric data concurrent with the hydrothermal data. When fully processed, the DSL-120 data will yield complete and precise maps of not only the location and depth of the axial

graben/caldera, but maps of other fault and fissure patterns as well. These data sets will provide an unprecedented opportunity to compare the distributions of permeability indicators and hydrothermal activity over a multi-segment ridge section [Hey *et al.*, 2001].

5. Plume Chemistry

In addition to producing detailed maps of the plume distribution, the tows and casts also yielded a densely sampled transect of the plume chemical composition along the ridge axis. While a detailed description of the chemical characteristics of each plume is beyond the scope of this paper, we can outline the range of plume chemistries sampled and identify at least 14 distinct plume regions that point to specific hydrothermal source areas on the ridge axis (Table 1). These observations also provide insight into the magmatic state of the RAPA NUI area.

The magmatic state of a ridgecrest can affect the chemistry of hydrothermal discharge by modifying the degree of volatile outgassing. In general, vent fields perturbed by recent (e.g., within $\sim 1\text{--}3$ yr) magmatic activity discharge fluids with higher volatile/metal ratios than more mature fields [e.g., Mottl *et al.*, 1995; Urabe *et al.*, 1995; Butterfield *et al.*, 1997]. To look for evidence of recent magmatic activity in the RAPA NUI area, we measured both volatile and metal species in the plumes (see Appendix 1). Volatile species include $\Delta p\text{H}$, ^3He , particulate sulfur (as an indicator of H_2S), and CH_4 . We measured a wide range of dissolved and particulate metal species, and here we concentrate on total dissolvable (TD) Fe and Mn as primary hydrothermal indicators. The data set we discuss (Figure 7) includes the plume-maximum sample from each on-axis vertical cast, plus all tow samples within the typical depth range of the plume horizon. (^3He data is available only from a smaller subset of the vertical casts.) The tows concentrated on obtaining regularly spaced samples between and within plume maxima along each segment.

Each of these tracers offers insight into the chemical and geological processes taking place at a given location. ^3He has a solely magmatic origin and thus its presence provides unequivocal evidence of magmatic activity [Lupton *et al.*, 1977]. $\Delta p\text{H}$ is a proxy for the concentration of CO_2 in the plume [Resing and Sansone, 1996; Resing *et al.*, 1999], and its excellent correlation with the concentration of ^3He in these samples ($r^2 = 0.80$) supports a largely magmatic origin of CO_2 as well. High concentrations of particulate sulfur (PS) (i.e., high PS/PFe ratios) have been observed almost exclusively at recently ($\lesssim 3$ yr) erupted sites rich in microbial debris and CH_4 [Urabe *et al.*, 1995; Feely *et al.*, 1996, 1999; McLaughlin-West *et al.*, 1999]. These high values may arise from magmatic outgassing of H_2S and either inorganic precipitation of the H_2S and/or microbially mediated PS formation. The origin of hydrothermal CH_4 is far more complex than that of other tracers, having at least four possible sources [Whelan, 1988]: outgassing of juvenile CH_4 , biological production, thermal breakdown of organic material at $>100^\circ\text{C}$, and inorganic synthesis at $>300\text{--}400^\circ\text{C}$. This combination of sources makes it difficult to ascribe the CH_4 distribution to a particular process. While observations of CH_4 in hydrothermal areas describe a consistent association between magmatic activity and CH_4 presence [Mottl *et al.*, 1995], not all eruptions have produced high CH_4 concentra-

tions. Plume CH_4 concentrations days and months after the 1996 Gorda Ridge seafloor eruption were surprisingly low (<10 nM), and demonstrate that significant quantities of CH_4 are not necessarily produced simply by water/rock reactions associated with a dike injection and eruption [Kelley *et al.*, 1998]. Fe and Mn are typically more concentrated in fluids from mature vent sites than in those from volatile-rich sites recently perturbed by magmatic activity [Butterfield *et al.*, 1997].

The along-axis distribution of each of these species shows a first-order correspondence with both the optical/thermal plume boundaries and the general trend of ridge inflation (Figure 7). For ΔpH , we found the highest concentrations north of $\sim 28.5^\circ\text{S}$ and south of $\sim 30.5^\circ\text{S}$ where A_{xs} is highest. This agreement implies a direct correlation between the rate of magma supply and gas concentrations in hydrothermal fluids. While the pattern of PS/PFe is more variable, many of the highest values also occur north of $\sim 28.5^\circ\text{S}$ and south of $\sim 30.5^\circ\text{S}$. In addition, samples near 29.8°S , 30.1°S , and 30.9°S without high ΔpH values also had unusually high PS/PFe ratios. The 30.1°S location corresponds to very high CH_4 values, but the high PS/PFe values at 29.8° and 30.9°S are isolated samples with no corresponding increases in other tracers.

In general, CH_4 concentrations are similar to values measured in other chronic hydrothermal plumes not associated with recent volcanism along the EPR [Gharib, 2000]. The broad agreement between CH_4 and ΔpH suggests that outgassing of juvenile CH_4 is its dominant source here, but measurements of vent fluids from the Ridge Flux area show that other processes can also be active in a superfast-spreading environment. Charlou *et al.* [1996] found that while CO_2 concentrations were highest in low-chlorinity fluids, consistent with enrichment by phase separation, the highest CH_4 concentration was found in the one high-chlorinity vent fluid sampled. They attributed the lack of correlation between CO_2 and CH_4 to leaching of gabbroic rocks with CH_4 -rich inclusions. Thus $\Delta\text{pH}/\text{CH}_4$ ratios may vary sharply and unpredictably among vent fluids, and so among plumes, on the RAPA NUI ridgecrest as well.

We found three areas where ΔpH and CH_4 were poorly correlated. One is the ridge north of 28.2°S (segment W3), where ΔpH values were among the highest of the entire study area but concentrations of CH_4 were not correspondingly elevated. Measurements of carbon isotopes in plume CH_4 suggest that microbial oxidation in the water column cannot account for the low CH_4 concentrations [Gharib, 2000], implying instead a weak seafloor source there. But conflicting with this explanation is the fact that plume samples between 28° and 28.2°S yielded unusually high (>2) PS/PFe ratios. A similar disagreement between ΔpH and CH_4 occurred in a small plume near 30.7°S , where we found the highest ΔpH (and ^3He) anomalies of the cruise, no PS/PFe anomaly, and little CH_4 . In a third area near 30.1°S , a small but intense plume held not only the highest CH_4 values sampled (>20 nM) but also PS/PFe ratios >5 . Surprisingly, though, ΔpH values were negligible.

In contrast to these inconsistencies in the volatile distributions, TDMn and TDFe closely covaried on all segments (Figure 7). Each peak in metal concentrations corresponded to a peak in the optical plumes except at 28.7°S and 29.5°S where plumes were too small to noticeably affect the gridded plume distribution. In general, metal concentrations in

plumes over W3 and W4 were higher than over segments E3 and E4. Except for a few small plumes, the along-axis trends of TDMn and TDFe agreed with those of ΔpH and, except over segment W3, CH_4 . This general agreement sharply contrasts with results from the Ridge Flux section, where the pattern of CH_4 is anti-correlated with the PFe and dissolved (D) Mn variations, indicating a clear spatial distinction between volatile-rich and volatile-poor discharge sites (Figure 8).

Using these physical and chemical observations, we can identify at least 14 distinct plume regions that point to specific hydrothermal source areas on the ridge axis, including four vent sites precisely located by the observation of buoyant hydrothermal plumes (Table 1). Unnavigated camera tows were conducted at five of the plume site locations: 28.08° (segment W3), 28.7° (W4), 29.72° (E1), 31.15° (E3), and 31.83° (E4). No active discharge was observed on any camera tow. Animals, especially anemones, bivalves, and crabs (galatheid) were common, but we photographed no biological community of obviously hydrothermal character. The linear extent of these sources apparently ranges from kilometer-sized (or less) individual vent fields to near-continuous discharge zones stretching for tens of kilometers. The plume chemistry suggests that mature hydrothermal systems (low volatile/metal ratios) produce most of the vent fluids and that recent eruptions have been few. Even so, the physical and chemical differences among the plumes suggest an interesting diversity of sources on the seafloor. At three locations, for example, are plumes that fall clearly outside the limits of a “mature” hydrothermal source. High ΔpH and PS/PFe ratios found in samples near 28.1°S suggest recent eruptive activity or magmatic outgassing, although CH_4 concentrations are lower than expected for either process. At 30.1°S , both PS/PFe ratios and CH_4 concentrations are exceptionally high, while dissolved metal concentrations are low. Moreover, this plume had an intense ΔNTU signal but nearly undetectable $\Delta\theta$ (Figure 3). These characteristics are reminiscent of the 9.8°N EPR vent field, where a 1991 eruption produced high-volatile, low-metal, low-salinity fluids that created a plume with a high optical intensity but a low apparent $\Delta\theta$ due to hydrographic masking [Baker *et al.*, 1994; Lavelle *et al.*, 1998]. Finally, at 30.7°S the highest ΔpH and ^3He anomalies of the entire study area indicate a unique CO_2 - and ^3He -rich, metal-poor source.

What do these patterns in plume chemistry tell us about the current magmatic state of the RAPA NUI area and superfast-spreading ridge segments in general? For interpretative help we can look to other sites on the EPR with known or suspected recent eruptions where plumes have carried diagnostic chemical clues for at least months after an eruption. The most intensely studied such site is the 1991 eruption at $\sim 9.8^\circ\text{N}$ [Haymon *et al.*, 1993]. A plume study 6 months post-eruption found CH_4 concentrations up to 90 nM and CH_4/DMn ratios up to 10 [Mottl *et al.*, 1995], with accompanying PS/PFe ratios up to 10 [Feely *et al.*, 1994]. Similarly high CH_4/DMn ratios (>1) [Urabe *et al.*, 1995], CH_4 values (>70 nM) [Ishibashi *et al.*, 1997], and PS/PFe ratios (>1) [Urabe *et al.*, 1995; Feely *et al.*, 1996] in plumes centered near 17.5°S and 18.6°S in the Ridge Flux section (Figure 8) imply that magmatic activity occurred there not long before plume sampling in late 1993. Other eruptions on both intraplate [Stuben, 1992] and ridge-axis [McLaughlin-West *et*

al., 1999; *Resing et al.*, 1999] volcanoes have produced CH_4 values >200 nM and $\text{CH}_4/\text{DMn} >2$. Only the small Gorda Ridge eruption in 1996 failed to produce plumes with high CH_4 concentrations [*Kelley et al.*, 1998].

In the RAPA NUI area, neither CH_4 concentrations (generally <10 nM) nor CH_4/TDMn ratios (<0.5) offer convincing evidence of recent magmatic activity on the scale encountered along the Ridge Flux section. These low values are more typical of “mature” discharge where a volcanic imprint is no longer obvious [*Mottl et al.*, 1995; *Charlou et al.*, 1996; *Ishibashi et al.*, 1997]. Distinctively high ratios of trace metals to hydrothermal heat support this interpretation. TDFe/heat ratios were typically 2–4 nM/J, and TDMn/heat 0.5–1.5 nM/J throughout the RAPA NUI area. These values are similar to those from vent fluids and plumes over zones of no recent volcanic activity in the Ridge Flux area, while much lower metal/heat ratios characterized vent fluids and plumes interpreted as perturbed by recent magmatic activity [*Charlou et al.*, 1996; G.J. Massoth, unpublished data]. The best candidates for sites of recent eruptions are those at 28.1° , 30.1° , and 30.7°S with unusual volatile/metal ratios.

Despite the scarcity of evidence for recent eruptions, the broad trend in $^3\text{He}/\text{heat}$ ratios points to significant differences in the magma supply rate among segments. This inference rests on the sensitivity of the $^3\text{He}/\text{heat}$ ratio in vented fluids and plumes to changes in magmatic activity. Ratios from magmatically dormant sites are typically $0.5\text{--}1 \times 10^{-8}$ nM/J but in plumes over recent eruptions have ranged as high as 4.7×10^{-8} nM/J (and up to $\sim 100 \times 10^{-8}$ nM/J in fluids from volatile-rich hotspot volcanoes) [*Lupton et al.*, 1989]. Theoretical calculations [*Lupton et al.*, 1989] indicate an average upper mantle $^3\text{He}/\text{heat}$ ratio of $\sim 2 \times 10^{-8}$ nM/J, and if heat and helium are not fractionated during transport in the upper mantle this value should represent the long-term average of midocean ridge hydrothermal fluids. In the RAPA NUI area, the $^3\text{He}/\text{heat}$ ratios broadly follow the geological indicators of both long-term (u_s) and shorter-term (A_{xs}) magmatic budget. The ratios rise above 2×10^{-8} nM/J over superfast-spreading and inflated segments and fall below 1×10^{-8} nM/J over the slower-spreading, weakly inflated propagator tips (Figure 7). Thus even though no large vent fields appear to have been in a recent post-eruptive state in early 1998, magma replenishment on most segments has been rapid enough to maintain a $^3\text{He}/\text{heat}$ ratio in balance with upper-mantle magma.

6. Conclusions

These data from the RAPA NUI survey, when combined with earlier results from the Ridge Flux survey, provide a comprehensive view of the correspondence between hydrothermal activity and ridge morphology along 1100 km of superfast-spreading ridge crest. We summarize our results by addressing the questions posed at the outset of this paper.

1. We found the spatial density of venting not appreciably different along the presumably “stable” ($13.5^\circ\text{--}18.7^\circ\text{S}$) and “unstable” ($27.5^\circ\text{--}32.3^\circ\text{S}$) superfast plate boundaries surveyed. While there is compelling evidence for ongoing reorganization of the plate boundaries in the RAPA NUI area [*Naar and Hey*, 1991; *Hey et al.*, 1995; *Korenaga and Hey*, 1996; *Martínez et al.*, 1997], this activity has not engendered a permanent increase in hydrothermal activity relative

to other superfast-spreading ridges. In particular, the propagator tips hosted negligible activity, similar to the Galapagos 95.5°W propagator [Hey *et al.*, 1992]. Hydrothermal activity there is likely short-lived and closely tied to infrequent pulses of magma supply.

2. Hydrothermal activity is sensitive to variations in the apparent magmatic budget at a variety of scales. At the multisegment scale, plumes cover ~60% of superfast-spreading (>130 km/Myr) ridgecrest in the two survey areas but <10% of the remaining, slower-spreading, axis. At the subsegment scale, hydrothermal plumes are commonly centered over peaks in ridge inflation. While relationships between ridge inflation and plume intensity at the kilometer scale [e.g., Hooff *et al.*, 1997], or average ridge inflation and plume incidence at the segment scale [e.g., Baker, 1996], are weak, a new approach used here does support a significant correlation between hydrothermal activity and ridge inflation. We show that the likelihood of a hydrothermal plume overlying a given 0.03°-long interval of ridgecrest increases linearly and significantly with increasing ridge inflation. Still unclear, however, is the extent to which along-axis variations in crustal permeability can modify the influence of magmatic heat in positioning hydrothermal vent fields.

3. In contrast to the Ridge Flux study, the RAPA NUI survey detected no extensive areas of volatile-rich plumes symptomatic of recent magmatic perturbation or outgassing. Instead, the low volatile/metal ratios of most (though not all) plumes points to a preponderance of mature hydrothermal systems. Analysis of the temporal and spatial scales of axial eruptions [Perfit and Chadwick, 1998] suggests that fast-spreading ridges may experience frequent (1–10 yr intervals) but small eruptions, so the chemistry of discharged fluids can change rapidly. Time-series data from vents in the Ridge Flux area between 1993 and 1999, for example, have documented profound changes in fluid chemistry [Roe *et al.*, 1999; Ishibashi *et al.*, 1999]. Thus the general lack of volatile-rich plumes in the RAPA NUI area during our cruise is not likely characteristic of the long-term diversity of hydrothermal chemistry there. This view is supported by the 1999 discovery of extremely gas-rich, phase-separated fluids at 31.8°S [Lupton *et al.*, 1999], perhaps indicative of a magmatic intrusion more recent than our 1998 cruise. Even with a scarcity of recent magmatic perturbations, however, the broad correspondence between volatile tracers (such as ΔpH and $^3\text{He}/\text{heat}$) and proxies of magma supply (such as A_{xs} and u_s) identifies a pervasive magmatic imprint on this superfast-spreading group of ridge segments.

Appendix A: Methods

We used 34 conductivity-temperature-depth-optical (CTDO) vertical casts and 10 CTDO tow-yos to map optical, thermal, and chemical hydrothermal plumes. All CTDO casts used a high-precision Sea Bird 911plus CTD, a WET Labs light-backscattering sensor (LBSS), and a 20-bottle rosette [Baker and Urabe, 1996]. The sawtooth wavelength during tow-yos was typically 1–2 km.

In the deep Pacific, hydrothermal plumes are commonly identified, and their hydrothermal heat content estimated, by determining a hydrothermal temperature anomaly ($\Delta\theta$) at each depth z from an expression such as:

$$\Delta\theta(z) = \theta - (k_1\sigma_\theta(z) + k_2\sigma_\theta(z)^2 + b) \quad (\text{A1})$$

where $\theta(z)$ is potential temperature, $\sigma_\theta(z)$ is potential density, and k and b are regression coefficients for a first or second order fit of θ as a function of σ_θ immediately above the neutrally buoyant plume.

The LBSS measurement is a relative rather than absolute measure of the light backscattering and can differ slightly among individual LBSS instruments [Baker *et al.*, 2001a]. We report our results in terms of nephelometric turbidity units (NTUs) according to the expression

$$\Delta NTU = (V_r - V_b)/a_n \quad (\text{A2})$$

where ΔNTU = the plume LBSS anomaly above ambient water, V_r = the raw voltage reading of the LBSS, V_b = the sensor voltage in ambient water not affected by hydrothermal plumes, and a_n = a factor unique to each LBSS determined from a laboratory calibration using formazine [Baker *et al.*, 2001a]. There is a generally good fit between ΔNTU and particle mass concentration except in areas of recent seafloor volcanic activity where high levels of particulate sulfur and microbial debris in the water column apparently cause abnormally high backscattering values [Baker *et al.*, 2001a]. Temperature and optical anomalies were calculated from despiked 1 Hz CTDO data averaged into 10 s blocks.

Optical plumes were also mapped using as many as six self-contained Miniature Autonomous Plume Recorders (MAPRs) attached along the tow cable of the DSL-120 side-scan sonar (S.L. Walker *et al.*, Short-term variations in the distribution of hydrothermal plumes along a superfast-spreading center, 27°30'–32°20'S, submitted to *Earth and Planetary Science Letters*, 2001. Hereafter, Walker *et al.*, submitted.). MAPRs recorded temperature, pressure, and light-backscattering every 5 s, using the same type LBSSs as on the CTDO package. The DSL-120 tows also included an in-situ chemical analyzer mounted on the tow weight [Massoth and Hey, 1998; G.J. Massoth, unpublished data].

Shipboard methane analyses were modified from Brooks *et al.* [1981]. The cold trap, a 145-cm long column of 100/120 mesh Porapak QS, was submerged in ethanol cooled to –60°C. Analytical error was calculated at 2% from variations in the values given for standards, but a combined analytical and sampling error of about 8% was calculated from replicate samples. Subsequent laboratory experiments determined that the methane extraction efficiency was 67% [Gharib, 2000], and shipboard results were appropriately adjusted.

Total dissolvable trace metal samples were collected directly from Niskin bottles through Teflon petcocks into 250 mL I-ChemTM polyethylene bottles, then acidified with 1 mL of sub-boiling quartz distilled 6N HCl. Total dissolvable Mn was determined with a precision of ± 1 nM by modifying the direct injection method of Resing and Mottl [1992] by adding 4 g of nitrilo triacetic acid to each liter of buffer. Fe was determined with a precision ± 2 nM by modifying the method of Measures *et al.* [1995] for direct injection analysis.

pH samples were collected and pH determined as described previously [Resing *et al.*, 1999]. On the basis of measurements of pH in background casts and samples above the plume, this technique has a precision of 0.001 pH units within a single hydrocast and an overall daily precision and accuracy of 0.005 pH units. pH anomalies (ΔpH) are the difference between pH of a sample and the pH of water at the same density as the sample from a background profile. pH

anomalies can be related to CO₂ concentrations following the method of *Resing and Sansone* [1996] using the relation described by *Resing et al.* [1999].

Samples for helium analysis were drawn immediately after recovery of the CTDO/rossette package and sealed into copper tubing using a special hydraulic crimping device [*Young and Lupton*, 1983]. Helium concentrations and helium isotope ratios were determined on a 21-cm radius, dual-collector mass spectrometer. Precision of the ³He concentration measurements is 2×10^{-17} mol kg⁻¹.

Elemental composition of particulate matter was determined by x-ray primary- and secondary-emission spectrometry with a Rh source and Mo, Ti, Se, and Co secondary targets using a non-destructive thin-film technique [*Feely et al.*, 1991]. Precision averaged 2% for major elements except for sulfur (11%), and 7% for trace elements.

Cross-axis inflation (A_{xs}) is the cross-sectional area of the ridge axis above the reference depth (at 0.5 Myr) out to ± 8 km from the spreading axis, calculated following the method of *Scheirer and Macdonald* [1993] as modified by *Martínez et al.* [1997]. Net elevation is the height of the ridge axis above the reference depth. Both indices were calculated at 1 km intervals along each segment.

Acknowledgments. This research was funded by NSF RIDGE Program grants OCE-9529737 and OCE-9906896, and NOAA's VENTS Program. We thank the officers and crew of the R/V *Melville*, especially Bob Wilson, for support at sea. M. Davis, J. Gendron, R. Greene, G. Lebon, S. Maenner, Diana Pardee, D. Tennant, S. Walker, and the WHOI DSL-120 team led by Skip Gleason provided crucial assistance at sea and on-shore. RNH thanks Nancy Hulbert for graphics assistance. DFN acknowledges travel support from the University of South Florida Research Council. Contribution 2334 from NOAA/Pacific Marine Environmental Laboratory.

References

- Auzende, J.-M., V. Ballu, R. Batiza, D. Bideau, J.-L. Charlou, M.H. Cormier, Y. Fouquet, P. Geistdoerfer, Y. Lagabriele, J. Sinton, and P. Spadea, Recent tectonic, magmatic, and hydrothermal activity on the East Pacific Rise between 17°S and 19°S: Submersible observations, *J. Geophys. Res.*, *101*, 17,995–18,010, 1996.
- Baker, E. T., Geological indexes of hydrothermal venting, *J. Geophys. Res.*, *101*, 13,741–13,753, 1996.
- Baker, E. T., and T. Urabe, Extensive distribution of hydrothermal plumes along the superfast-spreading East Pacific Rise, 13°50'–18°40'S, *J. Geophys. Res.*, *101*, 8685–8695, 1996.
- Baker, E. T., Y. J. Chen, and J. Phipps Morgan, The relationship between near-axis hydrothermal cooling and the spreading rate of midocean ridges, *Earth Planet Sci. Lett.*, *142*, 137–145, 1996.
- Baker, E. T., M.-H. Cormier, C. H. Langmuir, and K. Zavala, Hydrothermal plumes along segments of contrasting magmatic influence, 15°20'–18°30'N, East Pacific Rise: Influence of axial faulting, *Geochem. Geophys. Geosys.*, *2*, Paper number 2000GC000165, 2001.
- Baker, E. T., R. A. Feely, M. J. Mottl, F. J. Sansone, C. G. Wheat, J. A. Resing, and J. E. Lupton, Hydrothermal plumes along the East Pacific Rise, 8°40' to 11°50'N: Plume distribution and relationship to the apparent magmatic budget, *Earth Planet. Sci. Lett.*, *128*, 1–17, 1994.
- Baker, E. T., D. A. Tennant, R. A. Feely, G. T. Lebon, and S. L. Walker, Field and laboratory studies on the effect of particle size and composition on optical backscattering measurements in hydrothermal plumes, *Deep-Sea Res.*, *48*, 593–604, 2001.
- Brooks, J., D. Reid, and B. Bernard, Methane in the upper water column of the northwestern Gulf of Mexico, *J. Geophys. Res.*, *86*, 11,029–11,040, 1981.

- Butterfield, D. A., I. R. Jonasson, G. J. Massoth, R. A. Feely, K. K. Roe, R. E. Embley, J. F. Holden, R. E. McDuff, M. D. Lilley, and J. R. Delaney, Seafloor eruptions and evolution of hydrothermal fluid chemistry, *Phil. Trans. R. Soc. Lond. A*, *355*, 369–386, 1997.
- Charlou, J. L., Y. Fouquet, J. P. Donval, and J. M. Auzende, Mineral and gas chemistry of hydrothermal fluids on an ultrafast spreading ridge: East Pacific Rise, 17° to 19°S (Naudur cruise, 1993) phase separation processes controlled by volcanic and tectonic activity, *J. Geophys. Res.*, *101*, 15,899–15,919, 1996.
- Feely, R. A., G. J. Massoth, and G. T. Lebon, Sampling of marine particulate matter and analysis by x-ray fluorescence spectrometry, in *Marine Particles: Analysis and Characterization*, edited by D.C. Hurd and D.W. Spencer, pp. 251–257, *Geophys. Monogr. Ser.*, *63*, AGU, Washington, D.C., 1991.
- Feely, R. A., E. T. Baker, K. Marumo, T. Urabe, J. Ishibashi, J. Gendron, G. T. Lebon, and K. Okamura, Hydrothermal plume particles and dissolved phosphate over the superfast-spreading southern East Pacific Rise, *Geochim. Cosmochim. Acta*, *60*, 2297–2323, 1996.
- Feely, R. A., E. T. Baker, G. T. Lebon, J. F. Gendron, J. A. Resing, and J. P. Cowen, Evidence for sulfur enrichment in hydrothermal particles at Axial Volcano following the January, 1998 eruption, *Geophys. Res. Lett.*, *26*, 3649–3652, 1999.
- Feely, R. A., J. F. Gendron, E. T. Baker, and G. T. Lebon, Hydrothermal plumes along the East Pacific Rise, 8°40' to 11°50'N: Particle distribution and composition, *Earth Planet. Sci. Lett.*, *128*, 19–36, 1994.
- Gharib, J., Methane in Hydrothermal Plumes Along the East Pacific Rise, 28–32°S, M.S. Thesis, Univ. Hawaii, Honolulu, 68 pp., 2000.
- Haymon, R. M., D. J. Fornari, K. L. Von Damm, M. D. Lilley, M. R. Perfit, J. M. Edmond, W. C. Shanks, III, R. A. Lutz, J. M. Grebmeier, S. Carbotte, D. Wright, E. McLaughlin, M. Smith, N. Beedle, and E. Olson, Volcanic eruption of the mid-ocean ridge along the East Pacific Rise at 9°45'–52'N: Direct submersible observations of seafloor phenomena associated with an eruption event in April, 1991, *Earth Planet. Sci. Lett.*, *119*, 85–101, 1993.
- Hey, R. N., J. M. Sinton, M. C. Kleinrock, R. N. Yonover, K. C. Macdonald, S. P. Miller, R. C. Searle, D. M. Christie, T. M. Atwater, N. H. Sleep, H. P. Johnson, and C. A. Neal, ALVIN investigation of an active propagating rift system, Galapagos 95.5°W, *Mar. Geophys. Res.*, *14*, 207–226, 1992.
- Hey, R. N., P. D. Johnson, F. Martínez, J. Korenaga, M. L. Somers, Q. J. Huggett, T. P. LeBas, R. I. Rusby, and D. F. Naar, Plate boundary reorganization at a large-offset, rapidly propagating rift, *Nature*, *378*, 167–170, 1995.
- Hey, R., E. Baker, J. Lupton, M. Kleinrock, F. Martinez, D. Naar, D. Bohnenstiehl, D. Pardee, G. Massoth, C. Rodrigo, S. Gegg, T. Reed, and A. Andersson, Fine-scale volcano-tectonic patterns along the hotspot and non-hotspot influenced fastest spreading parts of the East Pacific Rise, and their relation to hydrothermal activity, *Eos Trans. AGU*, *82*(47), Fall Meet. Suppl. Abstract T42C-0954, 2001.
- Hoof, E. E. E., R. S. Detrick, and G. M. Kent, Seismic structure and indicators of magma budget along the southern East Pacific Rise, *J. Geophys. Res.*, *102*, 27,319–27,340, 1997.
- Kelley, D. S., M. D. Lilley, J. E. Lupton, and E. J. Olson, Enriched H₂, CH₄, and ³He concentrations in hydrothermal plumes associated with the 1996 Gorda Ridge eruptive event, *Deep-Sea Res. II*, *45*, 2665–2682, 1998.
- Korenaga, J., and R. N. Hey, Recent dueling propagation history at the fastest spreading center, the East Pacific Rise, 26°–32°S, *J. Geophys. Res.*, *101*, 18,023–18,041, 1996.
- Ishibashi, J., H. Wakita, K. Okamura, E. Nakayama, R. A. Feely, G. T. Lebon, E. T. Baker, and K. Marumo, Hydrothermal methane and manganese variation in the plume over the superfast-spreading southern East Pacific Rise, *Geochim. Cosmochim. Acta*, *61*, 485–500, 1997.
- Ishibashi, J., U. Tsunogai, K. Okamura, D. A. Butterfield, K. Roe, G. J. Massoth, S. M. Maenner, and J. E. Lupton, Wide variation of CH₄/Mn ratios of high and low temperature fluids from southern EPR, *Eos Trans. AGU*, Fall Meet. Suppl., F1073–F1074, 1999.

- Lavelle, J. W., E. T. Baker, and G. J. Massoth, On the calculation of total heat, salt, and tracer fluxes from ocean hydrothermal events, *Deep Sea Res. II*, 45, 2619–2636, 1998.
- Lupton, J. E., E. T. Baker, and G. J. Massoth, Variable ^3He /heat ratios in submarine hydrothermal systems: Evidence from two plumes over the Juan de Fuca Ridge, *Nature*, 337, 161–164, 1989.
- Lupton, J., D. Butterfield, M. Lilley, J. Ishibashi, D. Hey, and L. Evans, Gas chemistry of hydrothermal fluids along the East Pacific Rise, 5°S to 32°S, *Eos Trans. AGU*, Fall Meet. Suppl., F1099, 1999.
- Lupton, J. E., R. F. Weiss, and H. Craig, Mantle helium in hydrothermal plumes in the Galapagos Rift, *Nature*, 267, 603–604, 1977.
- Lyle, M. W., M. Leinen, R. Owen, and D. K. Rea, Late Tertiary history of hydrothermal deposition at the East Pacific Rise, 19°S: Correlation to volcano-tectonic events, *Geophys. Res. Lett.*, 14, 595–598, 1987.
- Martínez, F., R. N. Hey, and P. D. Johnson, The east ridge system 28.5°–32°S East Pacific Rise: Implications for overlapping spreading center development, *Earth Planet. Sci. Lett.*, 151, 13–31, 1997.
- Massoth, G. J., and R. N. Hey, SUAVE perspectives on the Southern East Pacific Rise, *Eos Trans. AGU*, 79(45), F831, 1998.
- McLaughlin-West, E. A., E. J. Olson, M. D. Lilley, J. A. Resing, J. E. Lupton, E. T. Baker, and J. P. Cowen, Variations in hydrothermal methane and hydrogen concentrations following the 1998 eruption at Axial Volcano, *Geophys. Res. Lett.*, 26, 3453–3456, 1999.
- Measures, C. I., J. C. Yuan, and J. Resing, Determination of iron in seawater by flow injection analysis using in-line preconcentration and spectrophotometric detection, *Mar. Chem.*, 50, 3–12, 1995.
- Mottl, M. J., F. T. Sansone, C. G. Wheat, J. A. Resing, E. T. Baker, and J. E. Lupton, Manganese and methane in hydrothermal plumes along the East Pacific Rise, 8°40' to 11°50'N, *Geochim. Cosmochim. Acta*, 59, 4147–4166, 1995.
- Naar, D. F., and R. N. Hey, Tectonic evolution of the Easter microplate, *J. Geophys. Res.*, 96, 7961–7993, 1991.
- Owen, R. M., and D. K. Rea, Sea-floor hydrothermal activity links climate to tectonics: The Eocene carbon dioxide greenhouse, *Science*, 227, 166–169, 1987.
- Perfit, M. R., and W. W. Chadwick Jr., Magmatism at mid-ocean ridges: Constraints from volcanological and geochemical investigations, in *Faulting and Magmatism at Mid-Ocean Ridges*, *Geophys. Monogr. Ser.*, 106, edited by W.R. Buck, P.T. Delaney, J.A. Karson, and Y. Lagabriele, pp. 59–116, AGU, Washington D.C., 1998.
- Resing, J. A., and M. J. Mottl, Determination of manganese in seawater by flow injection analysis using online preconcentration and spectrophotometric detection, *Anal. Chem.*, 64, 2682–2687, 1992.
- Resing, J. A., and F. J. Sansone, Al and pH anomalies in the Manus Basin reappraised: Comments on the paper by T. Gamo et al., “Hydrothermal plumes in the eastern Manus Basin, Bismarck Sea: CH₄, Mn, Al and pH anomalies,” *Deep Sea Res. I*, 43, 1867–1872, 1996.
- Resing, J. A., R. A. Feely, G. J. Massoth, and E. T. Baker, The water column chemical signature after the 1998 eruption of Axial Volcano, *Geophys. Res. Lett.*, 26, 3645–3648, 1999.
- Roe, K. K., D. A. Butterfield, J. E. Lupton, and J. Ishibashi, Chemistry of hydrothermal fluids of the southern East Pacific Rise, 7°–32°S: Time-series and continued exploration, *Eos Trans. AGU*, Fall Meet. Suppl., F1073, 1999.
- Scheirer, D. S., and K. C. Macdonald, The variation in cross-sectional area of the axial ridge along the East Pacific Rise: Evidence for the magmatic budget of a fast-spreading center, *J. Geophys. Res.*, 98, 7871–7885, 1993.
- Schilling, J.-G., H. Sigurdsson, A. N. Davis, and R. N. Hey, Easter microplate evolution, *Nature*, 317, 325–331, 1985.
- Stuben, D., Manganese, methane, iron, zinc, and nickel anomalies in hydrothermal plumes from Teahitia and Macdonald volcanoes, *Geochim. Cosmochim. Acta*, 56, 3693–3704, 1992.
- Urabe T., et al., The effect of magmatic activity on hydrothermal venting along the superfast-spreading East Pacific Rise, *Science*, 269, 1092–1095, 1995.

- Whelan, J. A., Origins of methane in hydrothermal systems, *Chem. Geol.*, *71*, 183–198, 1988.
- Wilcock, W. S. D., and J. R. Delaney, Mid-ocean ridge sulfide deposits: Evidence for heat extraction from magma chambers or cracking fronts?, *Earth Planet. Sci. Lett.*, *145*, 49–64, 1996.
- Wright, D. J., R. M. Haymon, and D. J. Fornari, Crustal fissuring and its relationship to magmatic and hydrothermal processes on the East Pacific Rise crest (9°12' to 54'N), *J. Geophys. Res.*, *100*, 6097–6120, 1995.
- Young, C., and J. E. Lupton, An ultratight fluid sampling system using cold-welded copper tubing, *Eos Trans. AGU*, *64*, 735, 1983.

E. T. Baker, R. A. Feely, Pacific Marine Environmental Laboratory, NOAA, 7600 Sand Point Way NE, Seattle, WA 98115 (baker@pmel.noaa.gov; feely@pmel.noaa.gov)

R. N. Hey, F. Martinez, D. Pardee, Hawaii Institute of Geophysics and Planetology, University of Hawaii, Honolulu, HI (hey@soest.hawaii.edu, martinez@kiawe.soest.hawaii.edu)

J. E. Lupton, Pacific Marine Environmental Laboratory, NOAA, Hatfield Marine Science Center, Newport, OR (lupton@pmel.noaa.gov)

J. A. Resing, Joint Institute for the Study of the Atmosphere and Ocean, University of Washington, Seattle, WA (resing@pmel.noaa.gov)

F. J. Sansone, J. J. Gharib, Department of Oceanography, University of Hawaii, Honolulu, HI (sansone@soest.hawaii.edu)

M. Kleinrock, Department of Geology, Vanderbilt University, Nashville, TN (kleinrnc@ctrvax.vanderbilt.edu)

D. F. Naar, Department of Marine Science, University of South Florida, St. Petersburg, FL (naar@moontan.marine.usf.edu)

C. Rodrigo, Servicio Hidrografico y Oceanografico de la Armada Valparaiso, Chile

G. J. Massoth, Institute of Geological & Nuclear Sciences, Ltd., Gracefield Research Centre, PO Box 30-368, 30 Gracefield Rd., Lower Hutt, New Zealand (g.massoth@gns.cri.nz)

D. Bohnenstiehl, Lamont-Doherty Earth Observatory, 61 Rte 9W, Palisades, NY 10964 (del@ldeo.columbia.edu)

(Received _____.)

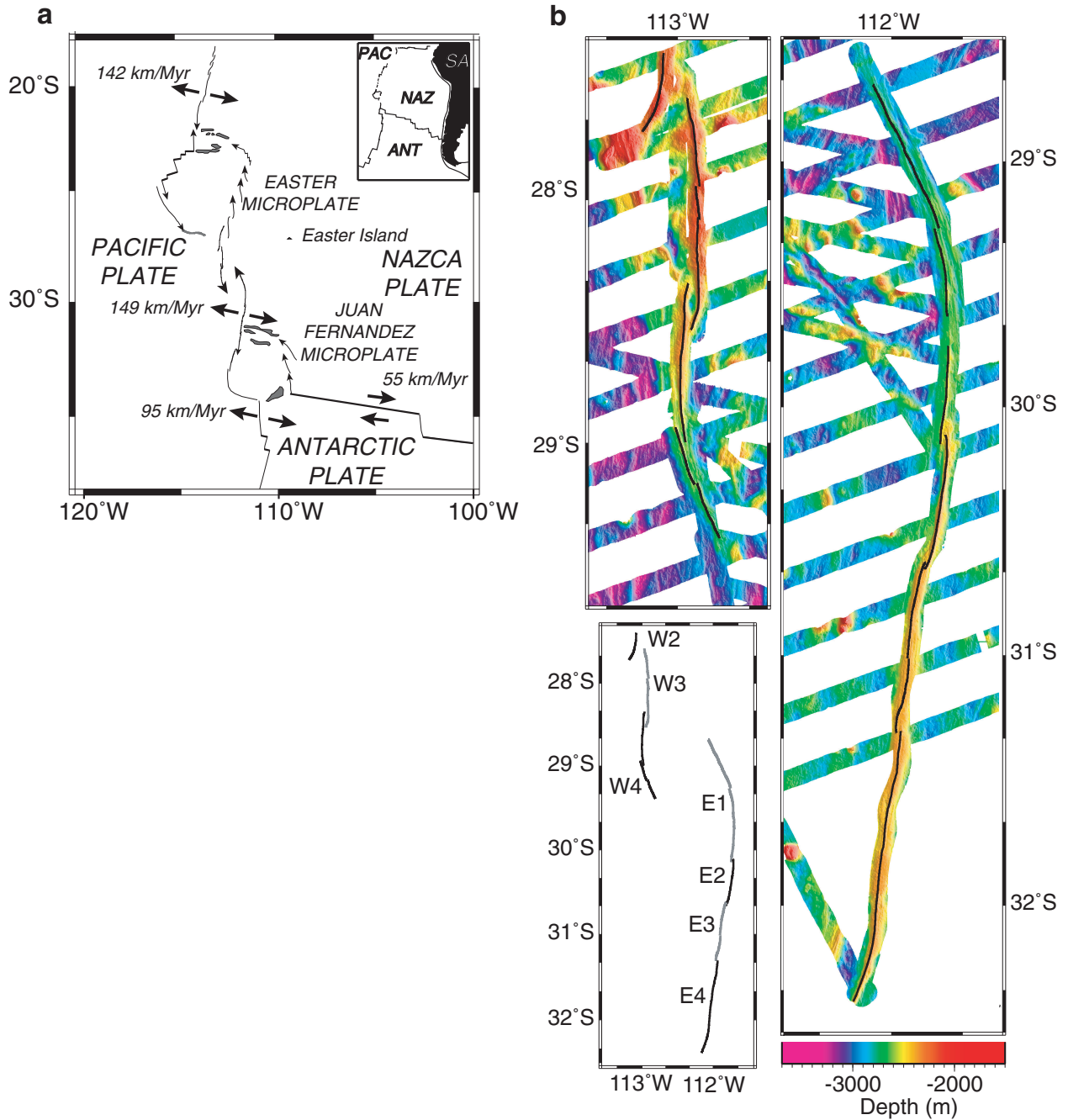


Figure 1. (a) Location map of the study region between the Easter and Juan Fernandez microplates in the southeast Pacific Ocean. Light lines are ridges, those with arrows are propagating. Heavy straight lines are transform faults. Double-headed arrows show axial spreading rates. (b) Ridgecrest bathymetry of the six segments surveyed, with black lines showing ridge axis. SeaBeam data from *Hey et al.* [1995] and *Martínez et al.* [1997] augmented by new data from our RAPA NUI cruise. Inset shows relative location of each second-order segment.

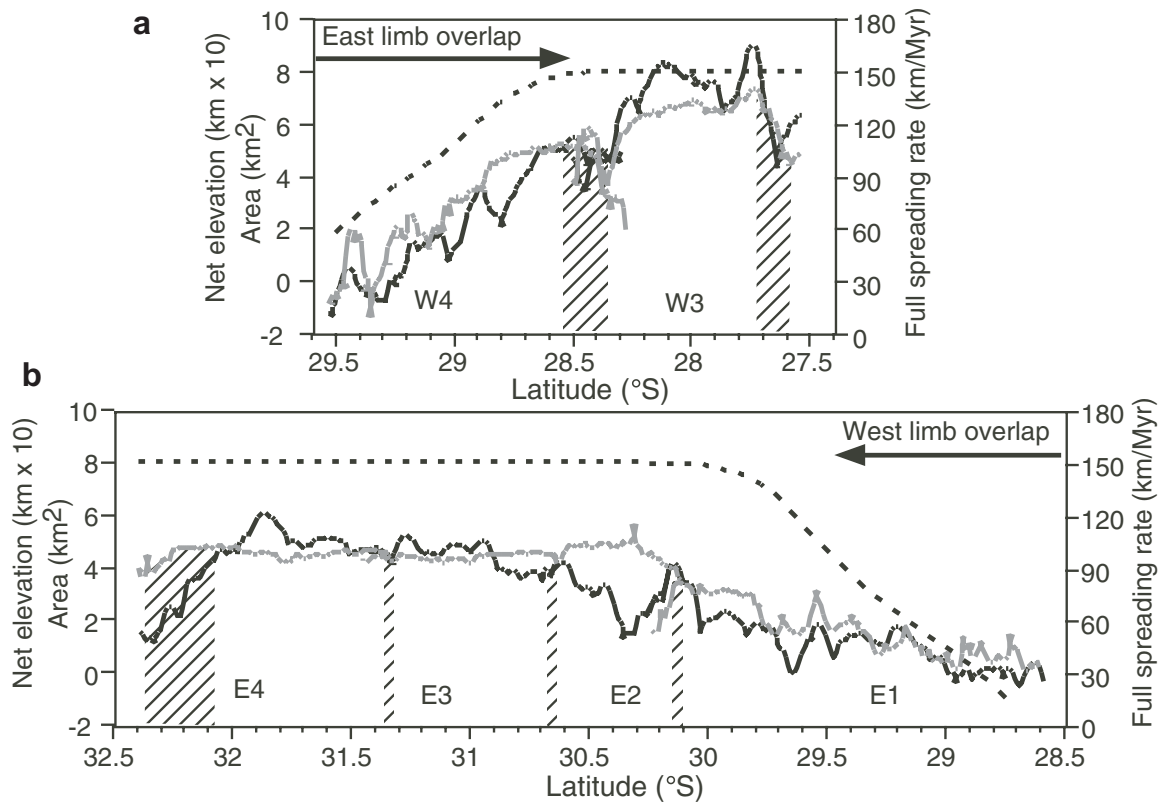


Figure 2. Along-axis trends in full spreading rate (dashed line), net elevation of the ridge axis (gray solid line), and the cross-sectional area of the ridge crest (dark solid line) for the west (a) and east (b) ridges. Extent of overlapping spreading centers separating each segment indicated by cross-hatched zones, and extent of the overlapping dueling propagators marked by arrows at the top of each panel.

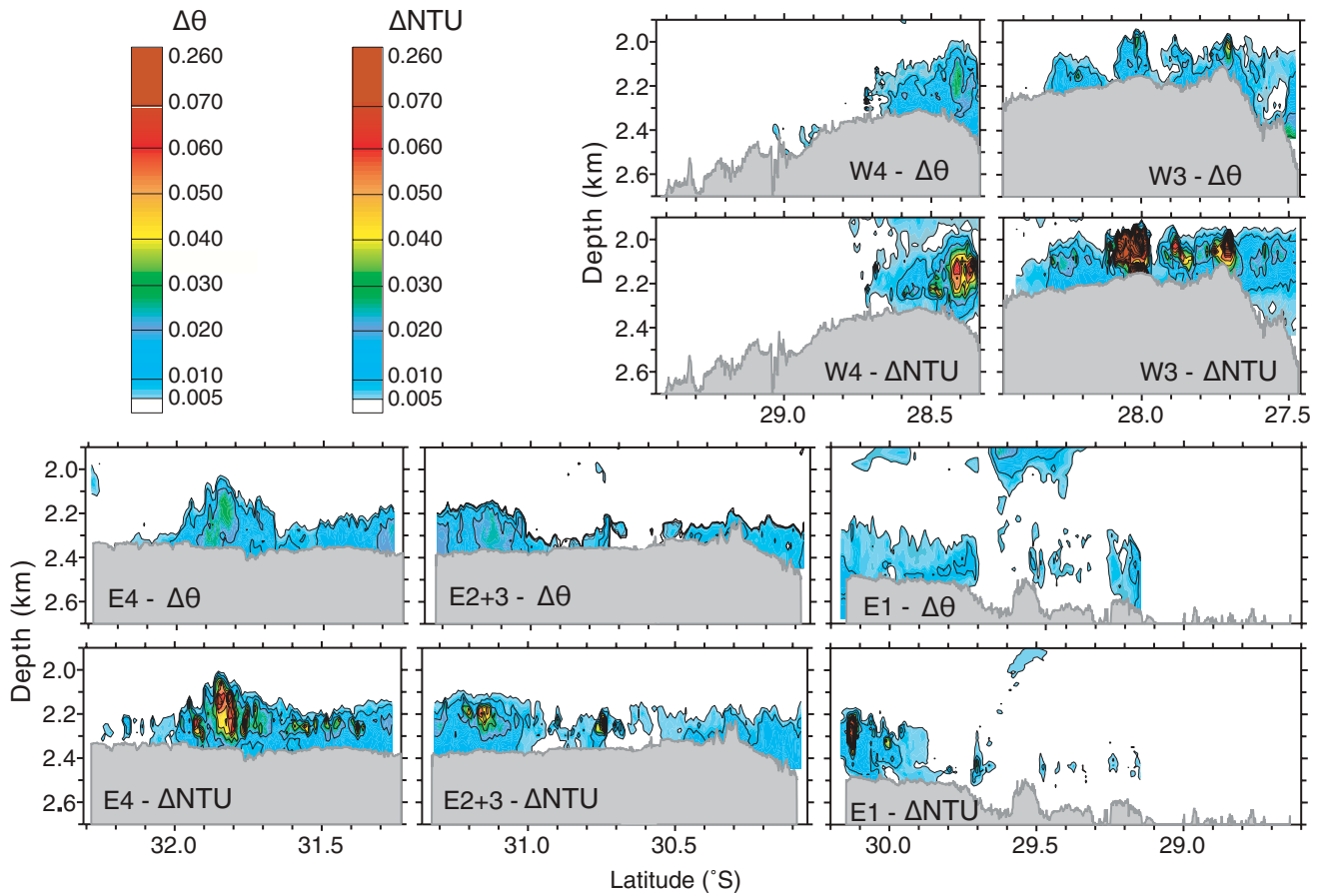


Figure 3. Segment-by-segment transects of hydrothermal plumes identified by temperature anomaly ($\Delta\theta^{\circ}\text{C}$) and light backscattering anomaly (ΔNTU) from CTDO tows. Lowest contour plotted for each variable is 0.005. CTDO tows extended south on the west ridge to 29.2°S and north on the east ridge to 29.14°S . Plume mapping using MAPRs attached to the tow line of the DSL-120 extended farther towards the tip of both the west (south to 29.35°S) and east (north to 28.65°S) ridges but no plumes were detected. Neither the $\Delta\theta$ nor ΔNTU signals north of $\sim 29.5^{\circ}\text{S}$ on E1 appear to be of hydrothermal character.

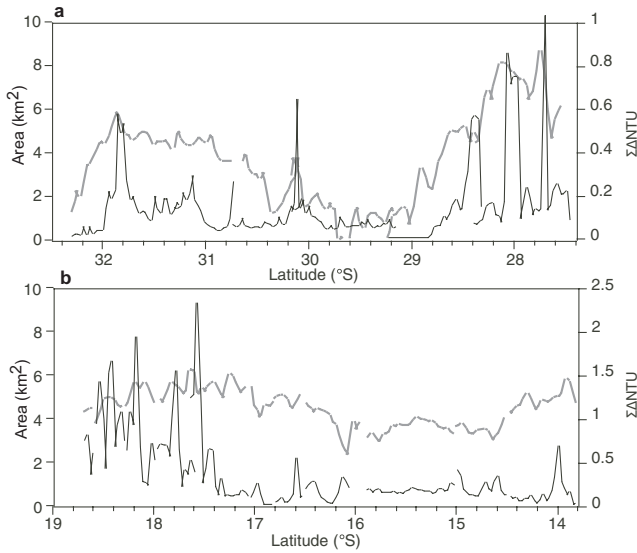


Figure 4. Comparison of along-axis ridge cross-sectional area (gray line) and vertically integrated ΔNTU ($\Sigma\Delta\text{NTU}$) at 0.03° latitudinal intervals (black line) for RAPA NUI (a) and Ridge Flux (13.5° – 18.7°S) (b) ridge sections. Note the tendency for peaks in $\Sigma\Delta\text{NTU}$ to occur near peaks in the cross-sectional area.

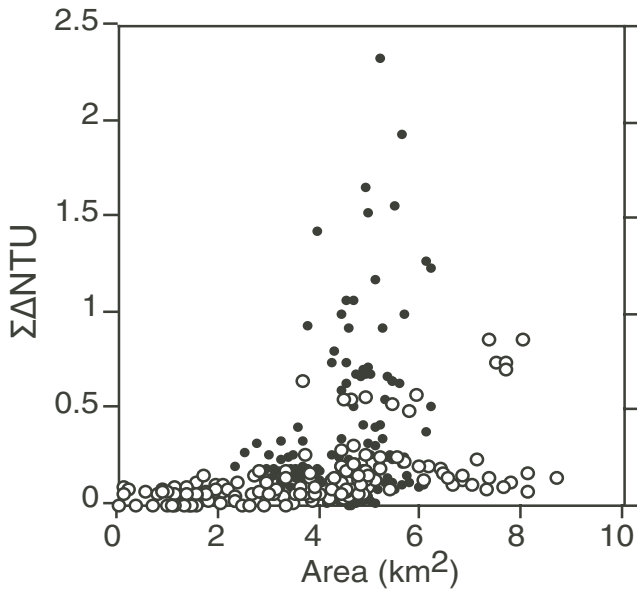


Figure 5. Scatter plot of cross-sectional area vs. vertically integrated ΔNTU at 0.03° latitudinal intervals for the Ridge Flux (solid circles) and RAPA NUI (open circles) areas. While there is no functional relationship between ridge inflation and plume optical inventory at this fine scale, intense plumes are found exclusively where $A_{xs} > 3.5 \text{ km}^2$.

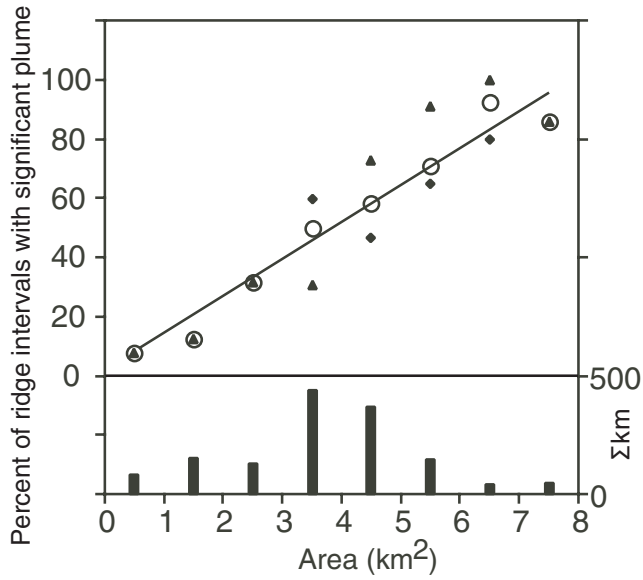


Figure 6. (Top panel) Scatter plot of binned cross-sectional area vs. percent of 0.03° axis intervals in each A_{xs} bin overlain by a significant plume ($\Delta NTU \geq 0.015$). For both the Ridge Flux (solid diamonds) and RAPA NUI (solid triangles) areas, and especially for the combined data ($r^2 = 0.94$) (open circles), there is a robust correlation between the likelihood of observing a hydrothermal plume and the local inflation of the ridge axis. Heavy line is least-squares fit to the combined data. (Bottom panel) Histogram of total ridge length in each A_{xs} bin for the combined data.

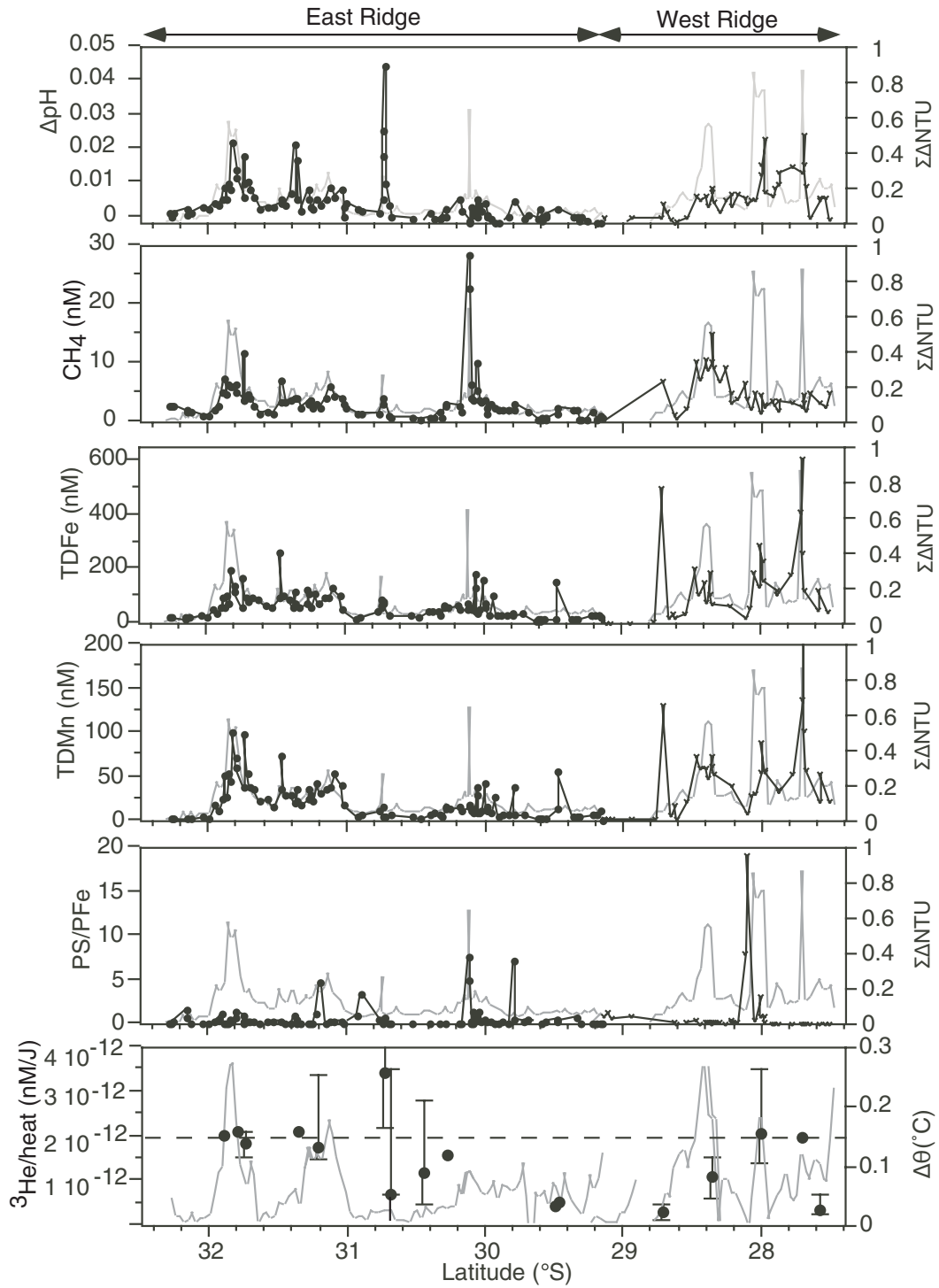


Figure 7. Along-axis trends in $\Sigma\Delta\theta\text{pH}$, CH_4 , TDFe , TDMn , PS/PFe , ${}^3\text{He/heat}$, $\Sigma\Delta\text{NTU}$, and $\Delta\theta$ from the RAPA NUI area. Solid circles and black line mark chemical data from the east ridge, crosses and black line mark chemical data from the west ridge, and gray line marks $\Sigma\Delta\text{NTU}$ data, except in bottom panel where $\Sigma\Delta\theta$ is plotted. Dashed line on the ${}^3\text{He/heat}$ plot marks the expected long-term average of midocean ridge fluids. Data set includes all tow samples within the plume horizon and plume maximum values from all vertical casts, but not isolated samples fortuitously tripped in highly concentrated near-bottom buoyant plumes. Note the generally good correspondence between concentration peaks in volatiles and metals.

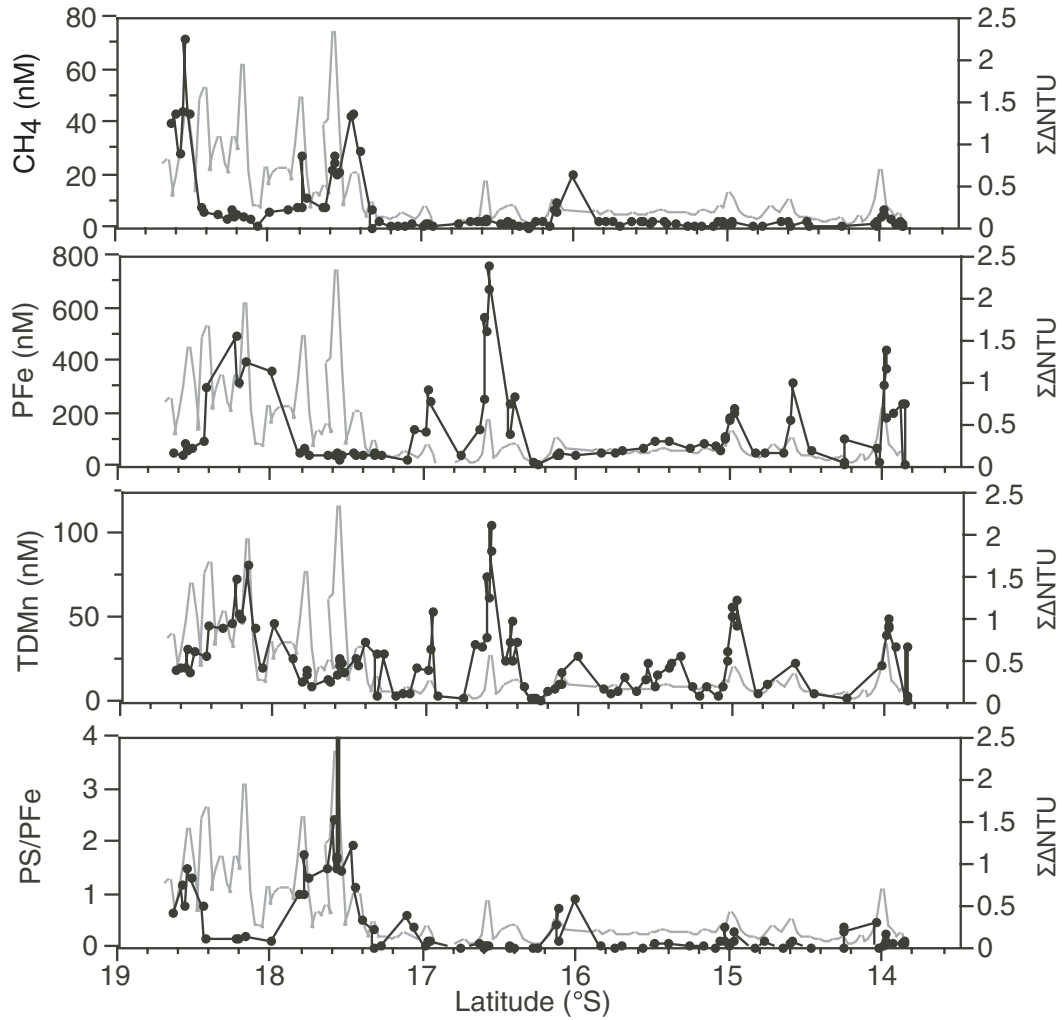


Figure 8. Along-axis trends in CH_4 [Ishibashi *et al.*, 1997], PFe [Feely *et al.*, 1996], DMn [Ishibashi *et al.*, 1997], and PS/PFe [Feely *et al.*, 1996] (solid circles and black line), and $\Sigma\Delta\text{NTU}$ (gray line) from the Ridge Flux area in 1993 (no ΔpH measurements were made during this cruise). Ridge Flux cruise measured DMn, not TDMn as on RAPA NUI cruise, but DMn accounts for >90% of total Mn [Ishibashi *et al.*, 1997]. Data set includes all tow samples within the plume horizon and plume maximum values from all vertical casts. Note that unlike the RAPA NUI area (Figure 7), trends in volatiles and metals were anti-correlated.

Table 1. Plume Characteristics and Vent Field Inferences

Location	$\Delta\theta$ ($^{\circ}\text{C}$)	CH_4 (nM)	ΔpH	TDFe (nM)	TDMn (nM)	Rise height (m)	Extent (km)	Comments
W3, 27.68 $^{\circ}$ –27.75 $^{\circ}$	0.04	3	0.02	400	150	150–200	15	Major field: high ΔpH , high-T, high metals
W3, 27.84 $^{\circ}$ –27.92 $^{\circ}$	0.02	3	0.015	100	30	175	10	Small field: high ΔpH , moderate metals
W3, 28 $^{\circ}$ –28.1 $^{\circ}$	0.032	3	0.02	300	80	200	20	Major field: very high ΔpH , high-T; high PS/PFe suggests recent venting/magmatic outgassing
W3, 28.2 $^{\circ}$ –28.3 $^{\circ}$	0.015	3	0.004	50	40	100	10	Small field: low ΔpH , low CH_4 , low metals, probably diffuse venting
W4, 28.35 $^{\circ}$ –28.5 $^{\circ}$	0.02	15	0.007	200	70	350	20	Major field: lower ΔpH but high CH_4 ; high plume rise suggests high-T vents
W4, 28.7 $^{\circ}$	0.02	7	0.003	500	130	175	2	Very small field: high metals, high CH_4 , low ΔpH ; buoyant plume detected
E1, 29.5 $^{\circ}$	0.01	2	0.002	150	60	?	?	Very small field?: based on only a single tow sample
E1, 29.7 $^{\circ}$ –29.8 $^{\circ}$	0.02	3	0.002	30	10	200	5	Small field: optical plume detected at 29.7 $^{\circ}$ S, buoyant plume at 29.8 $^{\circ}$ S
E1, 30.12 $^{\circ}$	0.01	25	0.002	50	15	250	3	Small field: based only on tow samples, very low ΔpH but high CH_4 , high PS/PFe suggests recent venting/magmatic outgassing
E2, 30.35 $^{\circ}$ –30.4 $^{\circ}$?	?	?	~90	~85	150	20	Small field: seen only on DSL-120 tow (no discrete samples, metal data from SUAVE)
E2, 30.7 $^{\circ}$ –30.85 $^{\circ}$	0.012	4	0.04	50	15	150	20	Small field: mainly diffuse, moderate CH_4 , low metals; buoyant plume detected at 30.82 $^{\circ}$ S
E3, 31.1–31.2 $^{\circ}$	0.025	5	0.005	100	50	200	15	Small field: low volatiles, moderate metals, probably some high-T venting; buoyant plume detected at 31.17 $^{\circ}$ S; high-temperature fluids sampled in January 1999 at 31.2 $^{\circ}$ S [Lupton <i>et al.</i> , 1999]
E3–E4, 31.2–31.6 $^{\circ}$	0.01–0.02	3–6	0.004–0.02	50–200	20–70	100	20	Large field: scattered mostly diffuse venting, variable in volatiles and metals
E4, 31.7–32.0 $^{\circ}$	0.03	10	0.02	200	100	325	35	Major field: multiple sources, hi-T venting, hi metals, hi CH_4 and ΔpH , but low PS/PFe; high-temperature fluids sampled in January 1999 at 31.8 $^{\circ}$ S [Lupton <i>et al.</i> , 1999]